Original Paper

Unsteady Analysis of Impeller-Volute Interaction in Centrifugal Pump

Kean Wee Cheah, Thong See Lee and Sonny H. Winoto

Department of Mechanical Engineering, National University of Singapore
9 Engineering Drive 1, Block EA, 07-08, Singapore 117576
g0500401@nus.edu.sg

Abstract

An unsteady numerical analysis has been carried out to study the strong impeller volute interaction of a centrifugal pump with six backward swept blades shrouded impeller. The numerical analysis is done by solving the three-dimensional Reynolds Averaged Navier-Stokes codes with standard k-ε two-equations turbulence model and wall regions are modeled with a scalable log-law wall function. The flow within the impeller passage is very smooth and following the curvature of the blade in stream-wise direction. However, the analysis shows that there is a recirculation zone near the leading edge even at design point. When the flow is discharged into volute casing circumferentially from the impeller outlet, the high velocity flow is severely distorted and formed a spiraling vortex flow within the volute casing. A spatial and temporal wake flow core development is captured dynamically and shows how the wake core diffuses. Near volute tongue region, the impeller/volute tongue strong interaction is observed based on the periodically fluctuating pressure at outlet. The results of existing analysis also proved that the pressure fluctuation periodically is due to the position of impeller blade relative to tongue.

Keywords: centrifugal pump, impeller, spiraling vortex flow, pressure fluctuation.

1. Introduction

A lot of emphasis has put on developing higher and higher efficiency pumps. This is because every percentage point of efficiency gained could bring significant energy saving and cost over the service life of the pumps. Traditionally, to design centrifugal pumps is mainly based on the steady-state theory, empirical correlation, combination of model testing and engineering experience. Pump design references by Stepanoff [1] and Gulich [2], are those good examples. However, engineers still need to have good understanding of the complex flow field and physics within the pump in order to further improve the pump performance. This is because flow field inside a centrifugal pump is very complex, three-dimensional and turbulent. Recirculation, separation, cavitation and unsteadiness also occur in such flow due to the curvature and rotation of the blades. In addition, the complex geometry of impeller, vaned or vaneless diffuser and spiral volute casing all will interact with each other and affect the overall pump characteristics and performances. Hence, extensive testing and huge amount of time and cost are required to improve the pump performance at design and off-design point operating conditions.

One of the flow phenomena within the radial flow impeller is the "jet wake" flow pattern developed near impeller exit. The flow separation in a centrifugal impeller normally occurs on the suction surface after leading edge and forms a wake flow on the suction side. This can be seen from measurement made by Eckartd [3] and Bwalya and Johnson [4]. The jet wake flow pattern is flow rate dependent and location of wake zone can changed significantly at impeller exit as demonstrated in measurement done by Howard and Kittmer [5], Murakami et al [6] and Hong et al [7].

The flow field inside the impeller at off-design condition is also very different from design point. The smooth and blade curvature congruent flow within the blade passages can changed to a stalled flow as reported by Pedersen et al [8] or becomes a significant flow separation as experimentally observed by Liu et al [9] and Abramian and Howard [10]. Other measurements done by Wuibaut et al [11], Westra et al [12], Visser [13], Choi et al [14] further demonstrated that flow field within impeller passages is highly complex and depends on flow rate, number of blades, blade curvature and specific speed as well.

There are many experimental studies on the effect of strong impeller volute interaction against the pump performance over the past. Dong et al [15] and Chu et al [16] used PIV measurement and found that jet-wake structures and pulsating flow near impeller exit. The orientation of the blades could affect the leakage and the pressure distribution. A vortex train generated as a result of non-uniform out fluxes from the impeller. Al-Qutub et al [17] experimental study on the radial gap showed that increasing the gap

reduces pressure fluctuations particularly in at part load conditions. The shape of the trailing edge shape also produced lower pressure fluctuations while maintaining the same performance. In addition, Dong [18] demonstrated that pump performance is not affected adversely by increasing the impeller and volute tongue gap up to 20% of impeller radius because of the reduces impact of non uniform out flux from the flow around the tongue and noise. The shape and location of the volute tongue also significantly affecting the pump performance such as the measurement done by Lipski[19]. Parrondo-Gayo et al [20] experiment with mounting of pressure transducers on front side of volute circumferentially around impeller outlet, found that pressure fluctuations and amplitudes are to be very dependent on both angular position and flow rate, maximum values corresponded to the tongue region for off-design conditions.

Knowing that there is a strong impeller volute tongue interaction, to improve further the pump performances at design and off-design operating conditions will be a tough challenge. However, with the advancing of computer power, significant improvement of numerical algorithms and more reliable CFD codes, it can be seen that there is an increasing trend of applying numerical methods to study the complex flow in a centrifugal and to improve the efficiency. Gulich [21] discussed the importance of three dimensional CFD in pump design and factors need to be considered in interpreting the results. A review by Horlock and Denton [22] suggested that the capabilities of CFD are continually improving and the future of turbomahcinery designs will rely even more heavily on it.

There are several numerical studies on the use of numerical method to predict the complex impeller and volute interaction based on two dimension models such as the one by Croba and Kueny [23] and Morfiadakis et al [24]. For three dimensional problem, Zhang et al [25,26], by solving the Navies-Stokes equations coupled with the standard two-equation k-ε turbulence model and their results compared well with those experimental study. He and Sato [27] also developed a three dimensional incompressible viscous flow solver and obtained satisfactory agreement with well established experimental data. Gonzalez et al [28] also validated the capability of CFD in capturing the dynamics and unsteady flow effects inside a centrifugal pump. In addition, with three dimensional numerical study, Gonzalez and Santolaria [29] able to find a plausible explanation for the flow structures inside the pump that is corresponding with the pressure and torque fluctuating values. Gonzalez et al [30], Spence and Amaral-Teixeira [31] even used three dimensional numerical computation and obtained good agreement between numerical and experimental results for double suction pumps.

The objective of present work is to numerically investigate the complex three-dimensional flow and to capture the dynamic and unsteady strong impeller volute casing interaction in a centrifugal pump at design point conditions near the impeller exit. This numerical investigation of the complex flow field inside a centrifugal pump can contribute to a better understanding of impeller-volute interaction. The centrifugal pump used in this study is consists of an impeller shrouded with six backswept blades, a curved intake section and a spiral volute casing. The specific speed, n_s of the centrifugal pump is 0.8574 and with a Reynolds number of 10^7 based on the impeller outer diameter and blade tip speed. The impeller inlet diameter d1, and outlet diameter, d_2 is 202 mm and 356 mm respectively. The impeller outlet width, b_2 is 46.8 mm. The flow from impeller is discharged into a spiral volute casing with mean circle diameter d^3 of 374 mm. The impeller is designed to operate at 1450 rpm with a flow coefficient, ϕ of 0.0244 and head coefficient, ψ of 0.1033 at best efficiency point.

Figure 1 shows the cross-section of the pump and the mid-plane is located at z/b = 0.5. Eight cross-sectional planes are cut in according to the various angular locations in volute casing for later discussion. Plane I at 0° is closest to volute tongue and the following Plane II to Plane VIII are spaced with an increment of 45° in anti-clockwise angular direction up to 315°. The impeller passages are labeled from 1 to 6 in anti-clockwise direction with Passage 1 closest to the volute tongue. Similarly, the impeller blades are labeled as Blade 1 to 6 in anti-clockwise direction with Blade 1 is between Passage 1 and Passage 6, Blade 2 is between Passage 1 and 2, and so on.
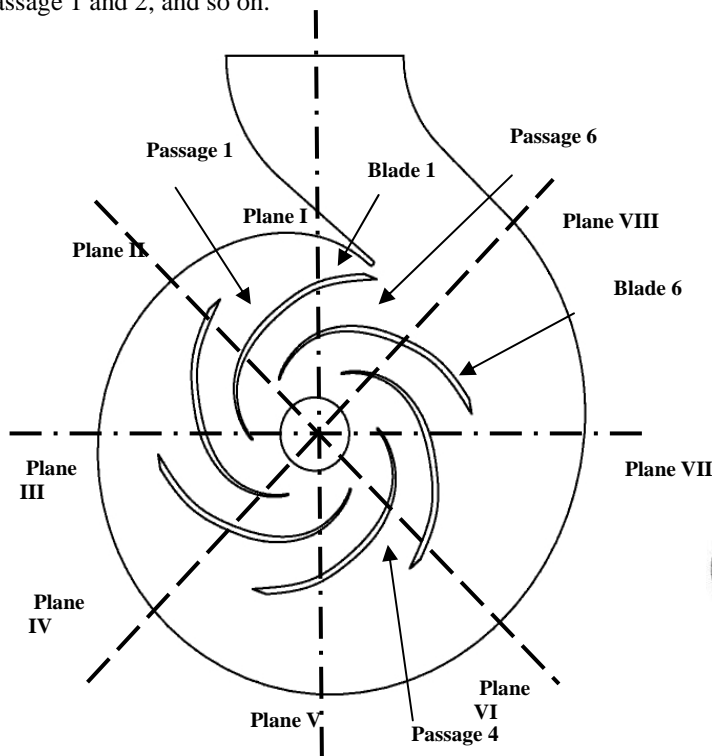

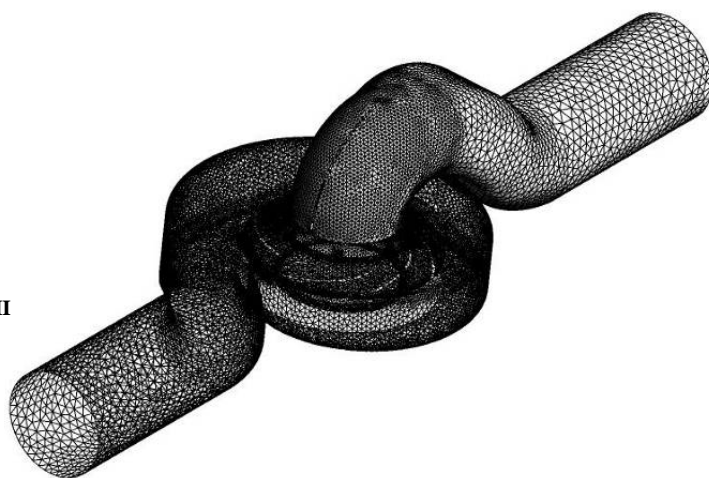**Fig. 1** Cross section view of the pump

Fig. 2 Mesh model of the pump

2. Numerical Model

In this numerical work, a commercially available CFD code, CFX 11.0 has been used to study the complex three-dimensional turbulent flow through the pump at design point. It is a general purpose CFD code solving three dimensional Reynolds Averaged Navies-Stokes (RANS) equations for steady and turbulent fluid flow. Many researchers have used this CFD code for numerical computation. The numerical results of Feng et al [32, 33] compared well with the PIV and LDV experiment results both qualitatively and quantitatively at different operating points.

In the present study, the standard k-ε turbulence model is used and the walls are modeled using a log-law wall function. For the numerical simulation, an unstructured tetrahedral meshing for all the computational domains is used. Figure 2 shows the mesh assembly of intake, impeller and volute sections. The meshes of three computational domains, the intake section, impeller and volute casing, are generated separately. The computation domains at the inlet of intake section and outlet of volute section are extended to allow recirculation. The extension is equal to two times of intake inlet and volute outlet diameter, which is same as the actual pressure measurement location in the test rig. A localized refinement of mesh is employed at regions close to volute tongue area, impeller blade leading and trailing edge in order to accurately capture the flow field structure. This is because the flow field properties variation such as pressure and velocity at these regions are expected to be substantial.

2.1 Steady and Unsteady Flow Computation

First, the whole pump is modeled and simulated under steady condition using wide range of flow rates. This is to obtain the overall results such as the pump characteristics and compare to the experimental results. Then unsteady numerical computation is carried out to capture the strong impeller volute interaction and flow dynamics.

The steady numerical computation is carried out with a multiple frames of reference (MFR) approach because the impeller flow field is with reference to a rotating frame whereby the volute casing and intake section refer to a stationary frame. The dissimilar meshes of the tetrahedral elements of intake section, impeller and volute that generated separately are connected by means of a "Frozen-Rotor" interface. For this kind of interface, the flow field variation across the interface is preserved. For steady calculations the relative position between impeller and volute casing modeled in the inter frames of reference is fixed in time and space. In this case, this Frozen-Rotor interface transfers the non axis-symmetric flow distribution developed only at the given relative position between the impeller and the stationary components to the neighboring region. Any circumferential flow distribution change due to the variation of the relative position between the impeller and volute casing is not considered in this interface. Although Frozen-Rotor interface is mainly used for the axis-symmetric flow problem, but the fast convergence of this model can save large computational time to obtain the overall pump performance curve for wide operating flow range. The numerical computation is considered converged when the maximum residual 10^{-4} is reached.

For the unsteady computation, the dissimilar mesh at the intake, impeller and volute interfaces are connected by means of "Transient Rotor-Stator" interface. For this interface, the surface fluxes of each side of the interface are first computed at the start of each time step at current relative position. The result from the steady state computation is used to initialize the unsteady computation.

3. Steady Analysis Results and Discussion

Before discussing any unsteadiness of flow field results within the pump, it is necessary to check some of the fundamental numerical setting that could be possibly affects the accuracy of the numerical results.

3.1 Inlet and Outlet Boundary Conditions

There are many ways to set the inlet and outlet boundary conditions for numerical simulation of fluid flow in a centrifugal pump. Table 1 shows a comparison of numerical result using different combination of inlet and outlet boundary conditions. There is a difference between outlet and opening type of boundary condition. If there is a flow recirculation at the boundary, the former one do not allows flow entrainment but the later one do allows the flow entrainment. Opening type of boundary condition is useful if there is recirculation and flow entrainment at the outlet of volute. For each set of boundary conditions, it is found that no significant difference for the solution to converge. The first type of boundary condition was chosen as it resembled to actual measurement where the inlet total pressure are known through measurement and the outlet pressure is measured in order to obtain the total pressure rise across the pump with various volume or mass flow rate.

Table 1 Boundary Conditions Study

Inlet	Outlet	Outlet Boundary Condition Type	ψ
Total Pressure	Mass Flow Rate	Outlet	0.0994
Mass Flow Rate	Total Pressure	Opening	0.0992
Mass Flow Rate	Mass Flow Rate	Outlet	0.0995
Mass Flow Rate	Static Pressure	Outlet	0.0992

3.2 y^+ and Mesh Sensitivity Study

To validate the accuracy of the numerical computation, it is important to study the y^+ and the mesh sensitivity of the computation domain. y^+ is defined as the dimensionless distance from the wall and is used to check the location of the first node away from a wall. The same mesh density and turbulence model is used to compare the influence of y^+ value.

The k-ε turbulence model is known to be unsuitable for low turbulent Reynolds number computations and ceases to be valid in the vicinity of near-wall region such as viscous sub-layer within the boundary layer flow, where viscous stress is dominant. Complex damping functions can be added to the k-ε model, as well as the requirement of highly refined near-wall grid resolution ($y^+ < 0.2$) in an attempt to model this kind of flow. This method often leads to numerical instability. In order to overcome this problem, the wall function approach is preferred to model the flow over near wall region. In this approach, the viscosity affected sub-layer region is bridged by employing empirical formulas to provide near-wall boundary conditions for the mean flow and turbulence transport equations. Hence, it is unnecessary to fully resolve the flow in this region. In the log-law region, the near wall tangential velocity is related to the wall-shear-stress τ_w, by means of a logarithmic relation, or also known to be log-law wall function. These formulas connect the wall conditions such as the wall-shear-stress to the dependent variables at the near-wall mesh node which is presumed to lie in the fully-turbulent region of the boundary layer. The major advantage of the wall function approach is that the high gradient shear layers near walls can be modeled with relatively coarse meshes, yielding substantial savings in computational time and storage. The log law of the wall is applicable for $20 < (y^+) < 300$ and the upper limit of y^+ is Reynolds number dependent. In this current study, the Reynolds number is in the order of 10^7 based on the impeller outer diameter and blade tip speed.

Table 2 y+ and mesh sensitivity study

y^+ Ave /Case	(a)	(b)	(c)	(d)	(e)
Pressure Side	357	314	250	186	121
Suction Side	381	314	249	184	120
ψ	0.0996	0.0995	0.0994	0.0994	0.0993

Comparison has been made for the centrifugal pump best efficient point with five different y^+ values within the impeller passage. The y^+ value is changed by adjusting the first node distance from the impeller blades wall while other mesh parameters and density is being kept constant. From Table 2, as the y^+ value decreasing, it shows that the head coefficient obtained at design flow rate with less than 0.5% difference for Case (a) and (e). Based on this, it can be said that the y^+ value is adequate for current study and does not have strong effect on the numerical result due the high Reynolds number for the flow within the impeller.

Table 3 Mesh sensitivity study

Mesh	(I)	(II)	(III)	(IV)	(IIV)
No. Nodes	88336	102903	122746	151866	190503
ψ	0.0996	0.0995	0.0994	0.0994	0.0993

To further confirm the mesh sensitivity, 5 cases with different impeller mesh level as shown in Table 3, were studied while keeping the volute casing and intake section mesh level constant, 114045 and 61211 nodes respectively. Again, there is no significant difference between the head coefficient obtained with different mesh levels. To minimize computation time, the computation of global pump characteristics is carried out using the mesh density of Case (IV), with 151866 nodes and with y^+ value about 250

3.3 Turbulence Models Comparison

The turbulence models selection and used in this centrifugal pump is based on the comparison of some of the widely used turbulence models in turbomachinery application, such as like k-ε, k-ω, RNG k-ε and Shear Stress Transport (SST) turbulence models. Two-equation turbulence model k-ε is widely used, as it offers a good compromise between numerical effort and computational accuracy. The RNG k-ε model is an alternative to the standard k-ε model. In general it offers little improvement compared to the standard k-ε model. The k-ω model does not involve the complex non-linear damping functions required for the k-ε model and considered to be more robust and more accurate. The k-ω based Shear-Stress-Transport (SST) model is highly accurate for prediction of the onset and the amount of flow separation under adverse pressure gradients by the inclusion of transport effects into the formulation of the eddy-viscosity.

In this study, the head coefficient is used to gauge the overall accuracy of the turbulence models while the pressure coefficient Cp on the blade is to compare the capability of the turbulence to model the flow characteristics and predict the onset of flow separation. The Cp is used for the numerical comparison as there is no actual experimental measurement to compare the accuracy of each turbulence model to predict the onset of flow separation. Fig. 3 shows the Cp on the impeller Blade 4 using different turbulence models. It can be seen that there is no significant difference among all the turbulence models.

Table 4 Turbulence Model Comparison

Turbulence Model	ψ
k-ε	0.0994
RNG k-ε	0.0984
k-ω	0.1007
SST	0.1003

From Table 4, it shows that the head coefficients obtained with different turbulence models are not significantly different. The k-ω turbulence model predicted highest head coefficient than other turbulence models and about 1.3% higher than the k-ε turbulence model. However, in terms of convergence speed, k-ε turbulence model is faster and more robust. In term of overall pump efficiency, k-ε turbulence model is still comparable to k-ω turbulence model with only 0.95% difference. As such, the standard k-ε turbulence model is chosen for this study.
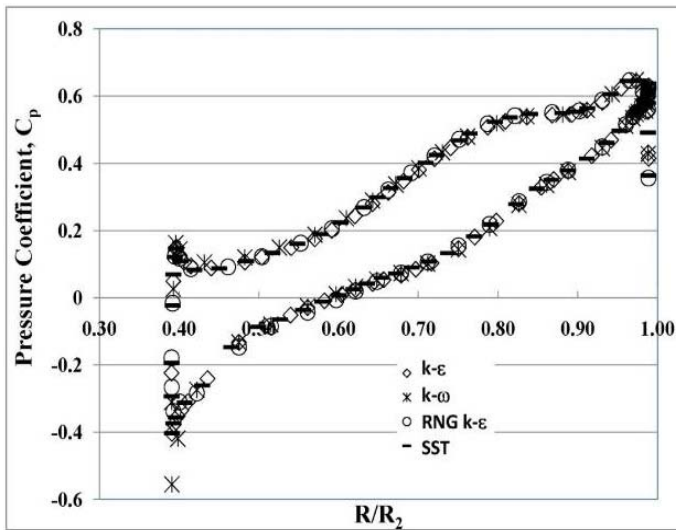
Fig. 3 Pressure coefficient on the blade
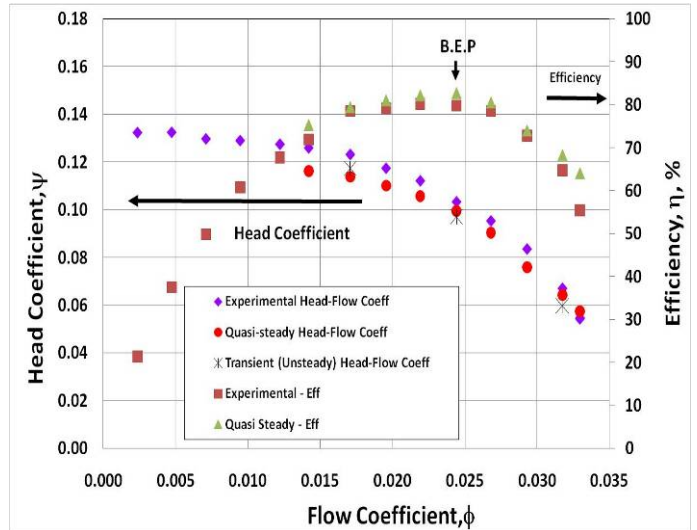
Fig. 4 Comparison of pump characteristics curves

3.4 Pump Performance

Prior to any discussion of the unsteady flow field developed in the pump, Fig. 4 shows a comparison of the numerical and experimental performance curves for the centrifugal pump. The numerical global characteristics curve is obtained by the steady computation. The numerically predicted pump characteristic curve by using steady flow computation over a wide flow range is in good agreement with the experimental results as discussed by Cheah et al [34].

At Q_{design}, the numerical predicted ψ is 0.099 as compared to the experimental ψ of 0.103, with a difference of about 4% at the best efficiency point. The numerical predicted efficiency is 82.71% but the actual pumps best efficiencies is at 79.86% only. In this case, the numerical predicted efficiency is higher that experimental one. This is because the numerical predicted efficiency only considered the torque within the rotating impeller without considering mechanical and leakage losses arise in the actual pump model. When modeling the centrifugal pump without side spaces and leakage path, the numerical torque is lower than measured shaft torque and this will increase the numerical efficiency of the centrifugal pump. If disk frictional and leakage losses are included, good agreement between numerical and experimental will be able to achieve.

The computation stopped at 60% of the Q_{design} due to convergence problem caused by large recirculation within the impeller passage and volute casing. At lower flow rate, the difference between the numerical and experimental result is slightly larger and it is believed that the numerical computation is over predicting losses incurred by the highly turbulent and recirculation flow inside the volute.

4. Unsteady Analysis Results and Discussion

The unsteady analysis is carried out after good agreement of the steady analysis pump performance curve is obtained. The result from the steady state computation is used to initialize the unsteady computation. In Fig 4, it shows that the unsteady analysis ψ is 0.097 as compared to steady analysis ψ of 0.0103. It can be said that the unsteady analysis is in good agreement with experimental ψ as well.

As the centrifugal pump operating under a relative high speed condition, the unsteady flow field developed due to impeller and volute tongue interactions is highly turbulent and unsteady. Hence, it is important to have sufficiently small time step resolution in order to capture the substantial flow field change. The time step size selected for numerical computation is affecting the accuracy and stability of the analysis. Different time step sizes have to be established to obtain satisfactory results

Three different time step of 6.8966×10^{-4}, 3.4483×10^{-4} and 2.2989×10^{-4} seconds that are equivalent to 6°, 3° and 2° blade rotation per time step are being studied. The steady result at the design point is used to initialize the unsteady computation and the global pump head coefficient is used to judge the convergence of results. From Fig. 5, it shows that the head coefficient fluctuates as the unsteady computation initiated from the steady solution. As the number of impeller revolutions increases, the global head coefficient reached a steady value. It can be said that at least 8 revolutions is needed to achieve a steady-state solution. For present study, the unsteady solution is obtained after 11 impeller revolutions.

The periodical global head coefficient is used to judge the time step size such that it is sufficient and able to capture the substantial flow field changes due to impeller-volute interaction. Fig. 6 shows the periodic fluctuating head coefficient plotted against the relative angular position of impeller Blade 1 from the volute tongue. Impeller Blade 1 trailing edge initially aligned with volute tongue at 0°. Relative angular position 0°, 60°, 120°, 180°, 240°, and 300° are where the impeller trailing edges are

aligned with the volute tongue. Since the impeller has six blades, the pitch of the trailing edge is 60°. At relative angular position of 30°, 90°, 150°, 210°, 270° and 330°, the volute tongue is positioned at between two trailing edges.

For 6° blade rotation per time step, the global head coefficient rise and lower smoothly and periodically. When the blade trailing edge is aligned with the volute tongue, the head coefficient is at minimum. While the volute tongue is positioned between the blade-to-blade trailing edges, the head coefficient is at maximum. However, for smaller blade rotation of time step size of 2° and 3°, the global head coefficient fluctuation shows a similar periodic behavior but captured additional information. The head coefficient is rising from lowest point and shows saddle point before reaching peak value. The saddle point before the peak is due to the highly unsteady flow discharged from the impeller exit. There is no significant head coefficient difference between blade rotation per time step of 2° and 3°. Based on this finding, 3° blade rotation or time step equivalent to 3.4483×10^{-4} second is used in current analysis as this time step is sufficient to capture the substantial flow field change. The total number of time step is 1320, which is equal to 11 revolutions of the impeller and the total time is 0.45517 second. The maximum number of iterations in each time step has been set to 10. This number of iterations is sufficient to reduce the maximum residuals by three orders of magnitude.
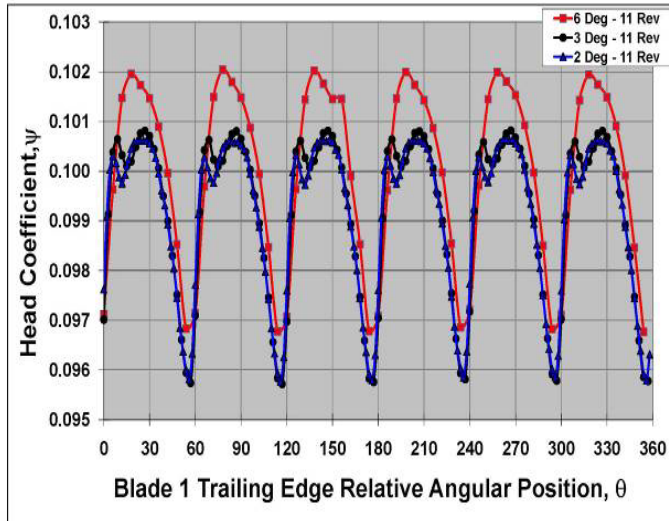

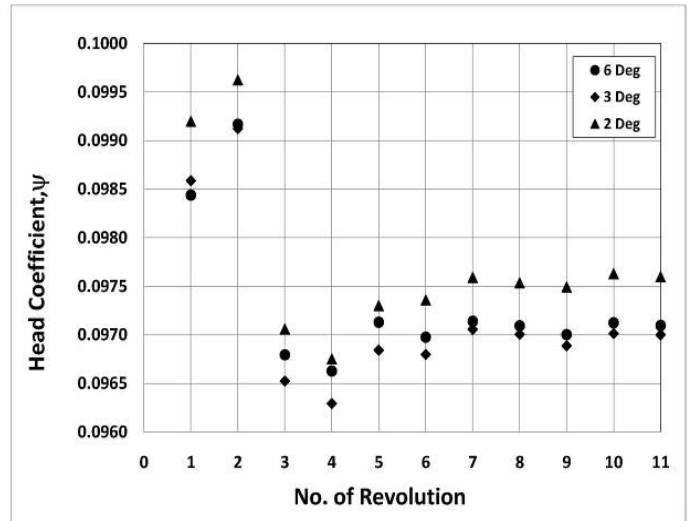**Fig. 5** Periodical head coefficient with relative angular position to volute tongue.

Fig. 6 Head coefficient convergence over number of impeller revolutions.

4.1 Unsteady Flow Field

Figure 7 shows the velocity vector inside the impeller at Q_{design}. The flow field inside the impeller passage is smooth and follows the curvature of the blades. However, there is a leading edge flow separation occurs on the suction side leading edge. Due to the unsteady effect developed at upstream of the curved intake section, the flow entering the passage is no longer tangential to the leading edge of impeller blade. The shockless velocity entry to impeller passage cannot be achieved even though at the best efficiency point. The leading edge flow separation stretch up to 15% of the blade cord length downstream. The recirculation flow behind the leading edge is experiencing a shearing effect exerted by the main flow in impeller passage and influences flow field in impeller passage in stream wise direction. A low flow zone is observed on the suction side towards downstream of near impeller exit. This phenomenon could be considered as jet-wake structure development phase as reported by many researchers.
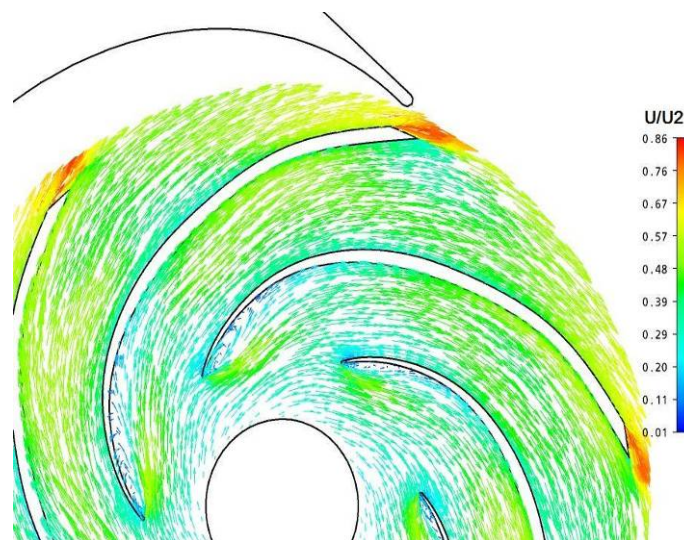

Fig. 7 Velocity vector at mid plane of impeller at Q_{design}.
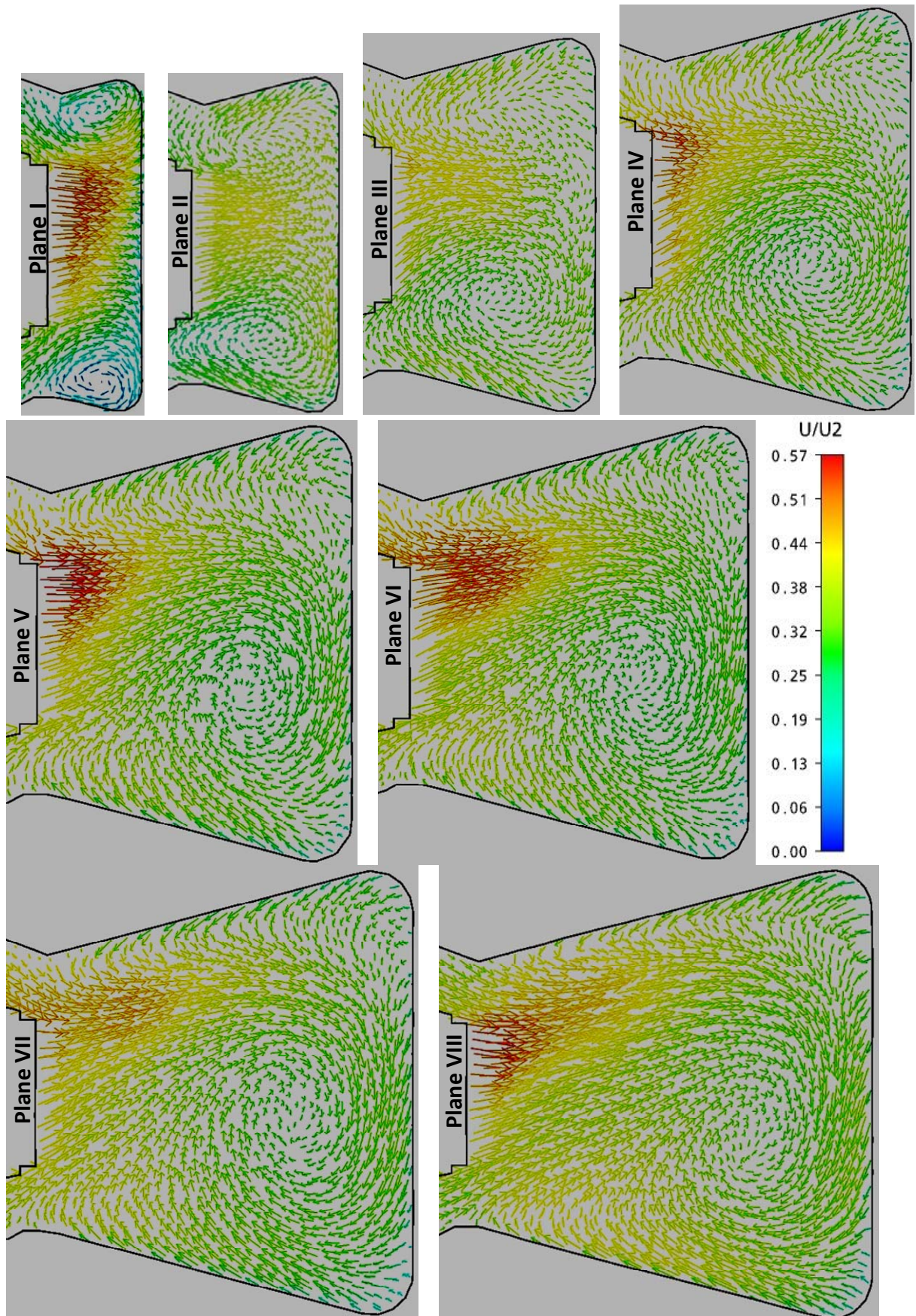
Fig. 8 Spiraling vortex formation inside the volute casing at different location.

As observed by Elhom and Alder [35] in the flow visualization, the incidence angle of the flow towards volute tongue is flow rate dependent. At high flow rate, a high positive flow incidence angle and with low flow, negative flow incidence angle at volute tongue. However, at optimum flow rate, zero incidence flow angle observed. Fig. 8 shows the flow pattern at the mid impeller

span, z/b=0.5 at volute outlet at Q_{design}. The flow collected in the volute casing flowing out smoothly at volute section. The flow incidence angle on volute tongue is almost zero. However, there still secondary flow observed at the mid section of the volute exit plane behind volute tongue. This is because the plane cut through the spiraling counter-rotating vortex flow starting from the volute tongue that seen in Fig. 8At Q_{design} when the flow is discharged into the volute as shown in Fig. 8, Plane I, a strong counter rotating vortex flow developed near volute tongue and evolving into symmetrical vortex flow in angular direction downstream. It can be noticed that the flow discharged from the impeller exit is jet flow like with a high speed core flow and retarded flow near shroud and hub. This high momentum core jet flow and shearing between the core and sides flow further enhanced the formation of the counter-rotating vortex formation and development. The confined volute flow passage profile at plane I to III and distorted velocity profile at impeller outlet as seen in Fig. 7 also attributed to this counter-rotating vortex formation flow. As the flow advancing in angular direction according to the cross-sectional plane with $\theta = 45°$, $90°$, $135°$, $180°$, $225°$, $270°$, $315°$ and finally at the exit plane, the symmetrical counter rotating vortex flow continue to develop. However, starting from Plane IV the jet flow core no longer at the center of the impeller exit and shifted to the shroud side. Because of this, the symmetrical counter rotating vortex flow is distorted with larger vortex core at lower corner of the volute casing. As the flow advancing in the angular direction towards the volute exit, the spiraling counter rotating vortex flow continues to evolve. The larger vortex at lower corner gained higher momentum by suppressing top corner vortex and forcing smaller vortex to disappear downstream.
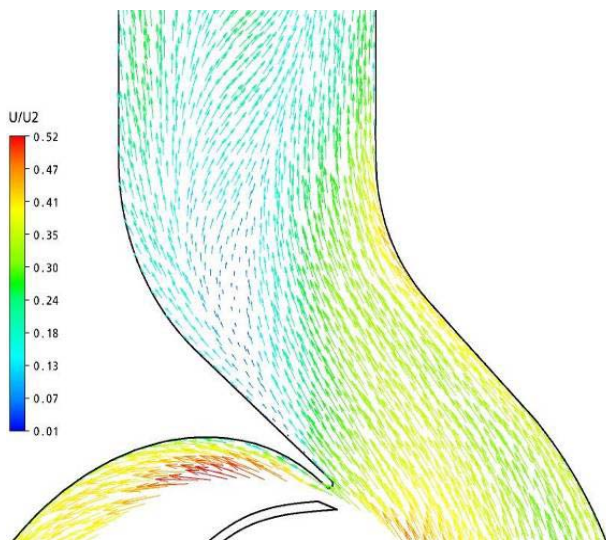

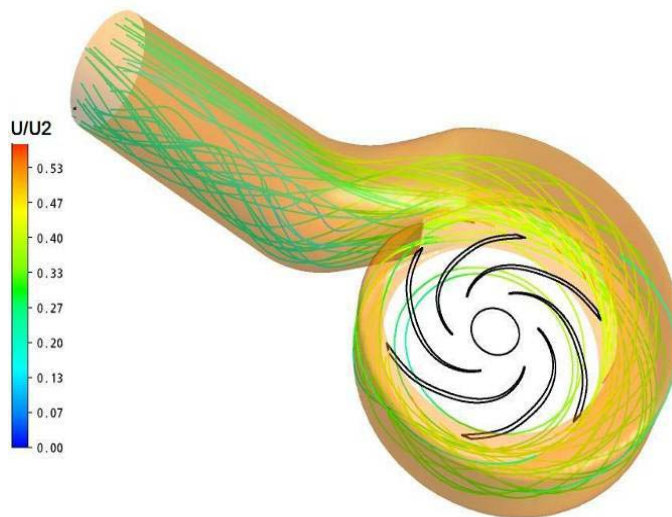**Fig. 9** Velocity vector near impeller exit

Fig. 10 Spiraling vortex flow inside the volute casing

To further visualize the spiraling vortex flow within the volute casing, Fig. 10 shows the stream line from impeller exit circumferentially to the volute exit. When the flow discharges from impeller into volute casing near volute tongue, the counter rotating vortex flow formed due to proximity of impeller trailing edge and volute tongue. As the flow advanced from volute tongue towards volute throat, the counter rotating vortex developed into spiraling vortex flow. After the volute throat, the spiraling vortex flow is retarded by the volute tongue and a wake or secondary flow is formed behind the volute tongue. Because of this volute tongue separation, the spiraling vortex flow split and no longer attached to the outer wall of volute, but instead attached to the inner of volute casing. It can be seen that the flow behind the volute tongue split into two region, with stratified flow attached to outer wall but spiraling vortex flow near inner volute. From here, significant mixing losses are expected.

4.2 Distorted Flow at Impeller Exit

Fig. 11 shows a series instantaneous non-dimensional meridional velocity at the impeller exit at Q_{design}. The frame is taken at a cut plane at the impeller exit Passage 6 with $r/r_2 = 0.99$. The figures are plotted according to the impeller trailing edge relative position to the volute tongue at Passage 1, 6 and 5 as indicated in Fig. 1. Passage 1 exit is closest to volute wall and tongue. Fig. 11 (a) to (f) shows the velocity profile at passage 6 at different angular position relative tongue. Fig. 11 (g) to (i) are for Passage 5 and Fig. 11(j) to (l) are for Passage 1. Flow discharge from Passage 6 will interact strongly with volute tongue as the impeller rotates. At $0°$, the suction side of impeller blade trailing edge is aligned to the volute tongue and for every time step or blade rotation of $6°$, a frozen frame is made. The volute tongue position is marked with dotted line as shown. In these series of frozen frames, it is clearly seen that evolution of the distorted velocity profile and jet/wake structure at impeller exit.

When the volute tongue rotates from $0°$ to $6°$, a clear wake flow core is observed near suction side at Passage 6. However, at Passage 5 and 6, the wake flow cores formed are near the suction shroud corner. As the impeller rotates further by $12°$, $18°$ and $24°$, the wake flow core is swept through by the volute tongue. The wake flow core will diffuse and breakaway. Another wake core is forming near the suction shroud corner when first wake flow core is carry downstream. As the impeller rotates further, the first wake flow core is diffused and the wake flow core formed will replaced it. The wake flow cores at Passage 1 and 5 are not totally affected by the volute tongue interaction.
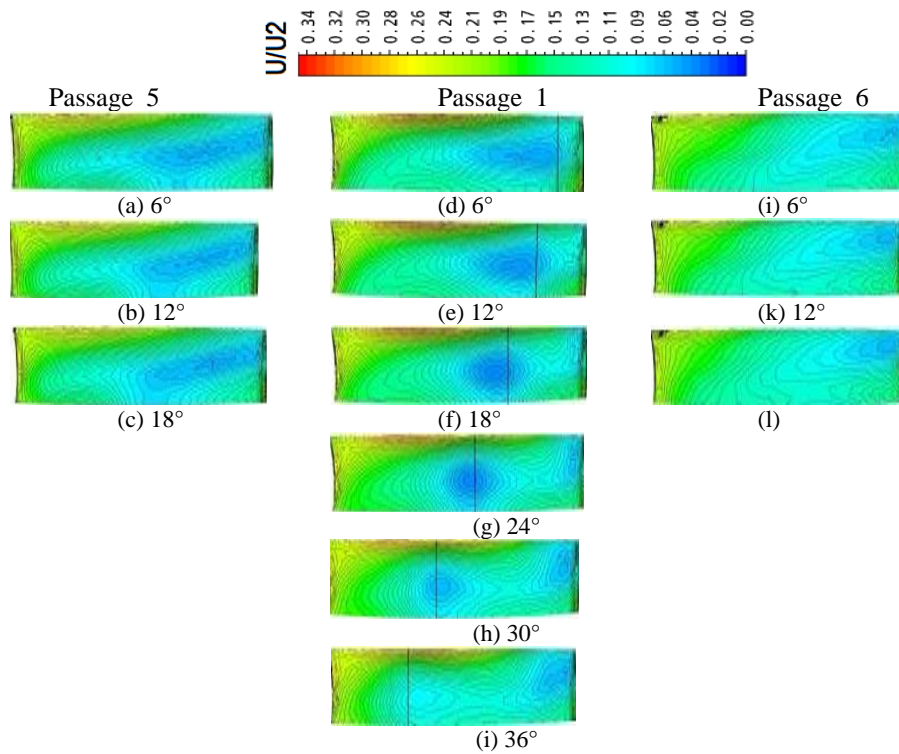
Fig. 11 Distorted impeller exit flow.

Fig. 12 shows the temporal and spatial static pressure distribution near volute tongue. The impeller is rotating in anti-clockwise direction. It can be seen that the isobar contours within the blade-to-blade overlap region are parallel and perpendicular to the blade pressure and suction sides. This is in good theoretical agreement where the pressure is increase in stream wise direction within the impeller passage. However, after the blade-to-blade overlap region, or so called the "throat" area, the isobar lines no longer smooth. The distorted isobar lines are the evidence of the instantaneous fluctuation pressure at the impeller periphery as seen in Fig. 6. As the impeller rotating in anti-clockwise direction, from -12° to +24° the distorted isobar lines are fluctuating around the impeller periphery line. These localized pressure fluctuation is affecting the global pump delivery head as well. As in Fig. 6 the pump delivery head is dependent on the location of the impeller trailing edge relative position with the volute tongue. The trailing edge and volute tongue have a localized high pressure envelop is due to the stagnation pressure point as well.
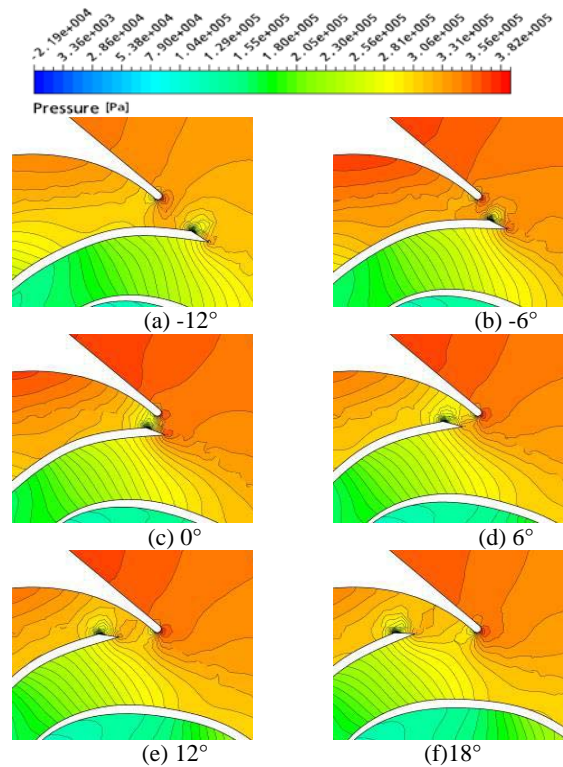

Fig. 12 Pressure contours at various relative volute tongue location.

Fig. 13 shows the pressure loading on the impeller blade at Q_design. The pressure coefficient Cp on the pressure and suction sides are plotted against the normalized radial direction with r/r2. There is a considerable pressure difference between the pressure and suction side. The pressure load increases along the cord length direction on either side of impeller blades. The pressure different on at Q_design is minimum at approximate 25% downstream of the leading edge and maximum after two third from the leading edge. From the suction side pressure loading on the blades, it can be concluded that there is a flow separation after leading edge where the static pressure is reduced up to a certain point. As the fluid flow downstream, there is a reattachment of the flow on the blade profile and this increase the wall pressure again. However, just after the overlap region at the trailing edge, it can be seen that the pressure different is reducing again because the flow on the suction and pressure sides trying to merge together. This because the blade loading is much depends on the curvature of the blade and thickness.
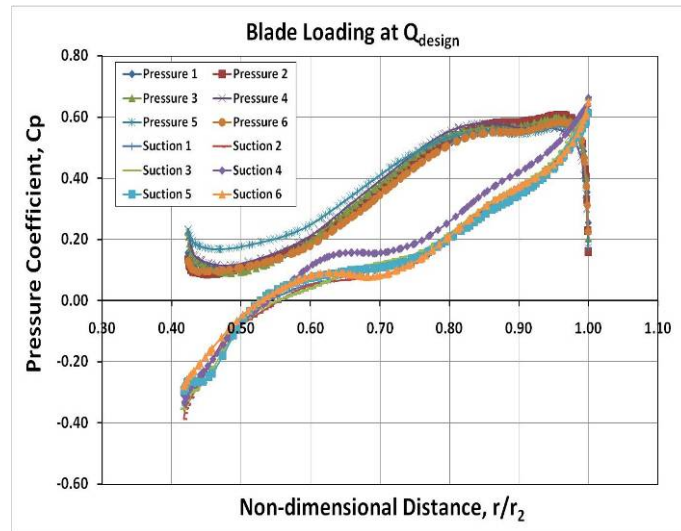

Fig. 13 Blade loading at on impeller blades

5. Conclusion

The complex centrifugal pump internal flow field and strong impeller volute interactions is studied numerically. At design point, the internal flow or velocity vector is very smooth along the curvature along the blades. However, flow separation developed at the leading edge due to non-tangential inflow conditions. The jet/wake flow structure is observed at the impeller exit where the wake core is located at the center of the passage and span across impeller exit. When the flow is discharged into volute casing circumferentially from the impeller outlet, the high velocity flow is severely distorted and formed a spiral flow pattern within the volute casing. The results of existing analysis proved that the pressure fluctuation periodically is due to the position of impeller blade relative to tongue and the flow field within the volute casing is always unsteady and turbulent.

Nomenclature

A	Cross-sectional Area [m^2]	Q	Volume flow rate [m^3/s]
b_2	Impeller outlet width [m]	r	Radius, radius of curvature [m]
c_p	Pressure coefficient$(=p-p_{atm}/ 0.5\rho U_2^2)$	U	Velocity [m/s]
d_1	Impeller outlet diameter [m]	U_{ave}	Mean velocity$(=Q/A)$
d_2	Impeller outlet diameter [m]	U_2	Blade tip velocity $(=\omega r)$
g	Gravity acceleration [m^2/s]	Re	Reynolds number $(=u_2d_2/v)$
H	Pump head [m]	n_s	Specific speed $(=N\sqrt{Q} / (gH)^{3/4})$
N	Rotation speed [rad/s]	v	Kinematic viscosity
p	Pressure	ψ	Non-dimensional head coefficient $(=gH/N^2d_2^2)$
		ϕ	Flow coefficient, $(=Q/Nd^3)$

References

[1] Stepanoff, A.J., 1957, "Centrifugal and Axial Flow Pumps: Theory, Design and Application," 2nd Ed. Krieger, Melbourne, FL.
[2] Gulich, J.F., 2008, "Centrifugal Pumps," Springer.
[3] Eckardt, D., 1975, "Instantaneous Measurements in the Jet-Wake Discharge Flow of a Centrifugal Compressor," ASME J. of Engineering for Power, 97(3), pp. 337-346.
[4] Bwalya, A.C., and Johnson, M.W., 1996, "Experimental Measurements in a Centrifugal Pump," ASME J. of Fluids Eng., Vol. 116, pp. 692-697.
[5] Howard J.H.G. and Kittmer C.W., 1975, "Measured Passage Velocities in a Radial Impeller with Shrouded and Unshrouded Configurations," ASME J. of Engineering for Power, pp. 207-213.

[6] Murakami M., Kikuyama K., and Asakura, 1980, "Velocity and Pressure Distributions in the Impeller passages of Centrifugal Pump," ASME J. of Fluids Eng., Vol.102, pp. 420-426.

[7] Hong S.S. and Kang S.H., 2002, "Exit Flow Measurement of a Centrifugal Pump Impeller," KSME International Journal, Vol. 16, No. 9, pp. 1147-1155.

[8] Pedersen, N., Larsen, P.S., and Jacobsen, C.B., 2003, "Flow in a Centrifugal Pump at Design and Off-Design Conditions – Part I: Particle Image Velocimetry (PIV) and Laser Doppler Velocimetry (LDV) Measurement," ASME J. of Fluids Eng., Vol. 125, pp. 61-72.

[9] Liu, C.H., Vafidis, C., and Whitelaw, J.H., 1994, "Flow Characteristics of a Centrifugal Pump," ASME J. of Fluids Eng., Vol. 116, pp. 303-309.

[10] Abramian, M., and Howard, J.H.G., 1994, "Experimental Investigation of the Steady and Unsteady Relative Flow in a Model Centrifugal Impeller Passage," ASME J. of Fluids Eng., Vol. 116, pp. 269-279.

[11] Wuibaut, G., Bois, G., Dupont, P., Caignaert, G., and Stanislas, M., 2002, "PIV Measurements in the Impeller and the Vaneless Diffuser of a Radial Flow Pump in Design and Off-Design Operating Conditions," ASME J. of Fluids Eng., Vol 124, pp. 791-797.

[12] Westra, R.W., Broersma, L., van Andel, K., and Kruyt, N.P., 2010, "PIV Measurements and CFD Computations of Secondary Flow in a Centrifugal Pump Impeller," ASME J. of Fluids Eng., Vol. 132, pp. 061104-1-8

[13] Visser, F.C., Brouwers, J.J.H., and Jonker, J.B., 1999, "Fluid Flow in a Rotating Low-specific-speed Centrifugal Impeller Passage," Fluid Dynamics Research, 24, pp. 275-292.

[14] Choi, Y.D., Kurokawa, J., and Matsui, J., 2006, "Performance and Internal Flow Characteristics of a Very Low Specific Speed Centrifugal Pump," ASME J. of Fluids Eng., Vol 128, pp. 341-349.

[15] Dong, R., Chu, S., and Katz, J., 1992, "Quantitative Visualization of the Flow within the Volute of a Centrifugal Pump. Part B: Results and Analysis," ASME J. of Fluids Eng., Vol. 114, pp. 396-403.

[16] Chu, S., Dong R., and Katz, J., 1995, "Relationship between Unsteady Flow, Pressure Fluctuations, and Noise in a Centrifugal Pump; Part B: Effects of Blade-Tongue Interactions," ASME J. of Fluids Eng., Vol. 177, pp. 30-35.

[17] Al-Qutub, A., Khalifa, A., and Khulief, Y., 2009, "Experimental Investigation of the Effect of Radial Gap and Impeller Blade Exit on Flow Induced Vibration at the Blade Passing Frequency in a Centrifugal Pump," Vol. 2009, Article I.D 704845.

[18] Dong, R., Chu S., and Katz, J., 1997, "Effect of Modification to Tongue and Impeller Geometry on Unsteady Flow, Pressure Fluctuations, and Noise in a Centrifugal Pump," ASME J. of Turbomachinery, Vol. 119, pp. 506-515.

[19] Lipski, W., 1979, "The Influence of Shape and Location of the Tongue of Spiral Casing on the Performance of Single Stage radial Pumps," Proc. Of 6th Conference Fluid Machinery, Budapest, pp. 673-680.

[20] Parrondo-Gayo J.L., Gonzalez-Perez J., and Fernandez-Francos, J., 2002, "The Effect of the Operating Point on the Pressure Fluctuations at the Blade Passage Frequency in the Volute of a Centrifugal Pump," ASME J. of Fluids Eng., Vol. 124, pp. 784-790.

[21] Gulich, J.F., 1999, "Impact of Three-dimensional Phenomena on the Design of Rotodynamic Pumps," Proc. Instn. Mech. Engrs., Vol. 213 Part C, pp. 59-70.

[22] Horlock, J.H. and Denton, J.D., 2005, "A Review of Some Early Design Practice Using Computational Fluid Dynamics and a Current Perspective," ASME J. of Turbomahcinery, Vol. 127, pp. 5-13.

[23] Croba, D. and Kueny, J.L., 1996, "Numerical Calculation of 2D, Unsteady Flow in Centrifugal Pumps: Impeller and Volute Interaction," Int'l J. For Numerical Methods In Fluids, Vol. 22, pp. 467–481.

[24] Morfiadakis, E. E., Voutsinas S. G., and Papantonis, D. E., 1991, "Unsteady Calculation in a Radial Flow Centrifugal Pump With Spiral Casing," Int'l J. For Numerical Methods In Fluids, Vol. 12, pp. 895-908.

[25] Zhang, M.J., Pomfret, M.J., and Wong, C.M., 1996, "Three-Dimensional Viscous Flow Simulation In A Backswept Centrifugal Impeller At The Design Point," Int'l J. of Computers & Fluids, Vol. 25, No. 5, pp. 497-507.

[26] Zhang, M.J., Pomfret, M.J. and Wong, C.M., 1996, "Performance Prediction of a Backswept Centrifugal Impeller At Off-design Conditions," Int'l J. For Numerical Methods in Fluids, Vol. 23, pp. 883-895.

[27] He, L., and Sato, K., 2001, "Numerical Solution of Incompressible Unsteady Flows in Turbomachniery," ASME J. of Fluids Eng., Vol. 123, pp. 680-685.

[28] Gonzalez, J., Fernandez, J., Blanco, E., and Santolaria, C., 2002, "Numerical Simulation of the Dynamic Effects Due to Impeller Volute Interaction in a Centrifugal Pump," ASME J. of Fluids Eng., Vol. 124, pp. 348-355.

[29] Gonzalez, J., and Santolaria, C., 2006, "Unsteady Flow Structure and Global Variables in a Centrifugal Pump," ASME J. of Fluids Eng., Vol. 128, pp. 937-946.

[30] Gonzalez, J., Manuel, J., Oro, M., Diaz, K.M.A. and Blanco, E., 2009, "Unsteady Flow Pattern for a Double Suction Centrifugal Pump," ASME J. of Fluids Eng., Vol. 131, pp. 071102-1-9.

[31] Spence, R., and Amaral-Teixeira, J., 2008, "Investigation into Pressure Pulsations in a Centrifugal Pump Using Numerical Methods Supported by Industrial Test," Computers & Fluids, Vol. 37, pp. 690-704.

[32] Feng, J.J., Benra, F.K. and Dohmen, H.J., 2007, "Numerical Investigation on Pressure Fluctuations for Different Configurations of Vaned Diffuser Pumps," International J. of Rotating Machinery, Vol. 2007, Article ID 34752.

[33] Feng, J.J., Benra, F.K., and Dohmen, H.J., 2009, "Comparison of Periodic Flow Fields in a Radial Pump among CFD, PIV, and LDV Results," International J. of Rotating Machinery, Vol. 2009, Article ID 410838

[34] Cheah K.W., Lee, T. S., and Winoto, S.H., 2011, "Numerical Study of Inlet and Impeller Flow Structures in Centrifugal Pump at Design and Off-design Points," International J. of Fluid Machinery and Systems, Vol. 4, No.1, pp. 25-32.

[35] Elholm, T., Ayder, E. and Van den Braembussche, R.A., 1992, "Experimental Study of the Swirling Flow in Volute of Centrifugal Pump," ASME J. of Turbomachinery, Vol. 114, pp. 366-372.